Solving coupled problems of lumped parameter models in a platform for severe accidents in nuclear reactors

Louis Viot, Laurent Saas, Florian de Vuyst

Solving coupled problems of lumped parameter models in a platform for severe accidents in nuclear reactors

Louis Viot[1,*]**, Laurent Saas** [2] **and Florian De Vuyst** [3]

[1]CMLA, Ecole Normale Supérieure de Cachan, 94235 Cachan, France

[*]email : louis.viot@cea.fr

[1,2]CEA, DEN, DTN/SMTA/LMAG, Cadarache, F-13108 Saint-Paul-lez-Durance, France

[3]LMAC, UTC, Sorbonne Universités, 60200 Compiègne, France

Abstract

This paper focuses on solving coupled problems of lumped parameter models. Such problems are of interest for the simulation of severe accidents in nuclear reactors : these coarse-grained models allow for fast calculations for statistical analysis used for risk assessment and solutions of large problems when considering the whole severe accident scenario. However, this modeling approach has several numerical flaws. Besides, in this industrial context, computational efficiency is of great importance leading to various numerical constraints. The objective of this research is to analyze the applicability of explicit coupling strategies to solve such coupled problems and to design implicit coupling schemes allowing stable and accurate computations. The proposed schemes are theoretically analyzed and tested within CEA's PROCOR platform on a problem of heat conduction solved with coupled lumped parameter models and coupled 1D models. Numerical results are discussed and allow us to emphasize the benefits of using the designed coupling schemes instead of the usual explicit coupling schemes.

Key words. *Severe Accidents, Multiphysics, Coupling Scheme, Partitioned Approach, Stability Analysis, Lumped Parameter Model, Complex System, Computing Efficiency*

Acronyms. *LP, lumped parameter; ECS, explicit coupling scheme; ICS, implicit coupling scheme*

1 Introduction

Mathematical and numerical resolution of coupled multiscale and multiphysics problems is a substantial issue arising in several engineering fields.

1

In particular in the field of severe accidents in nuclear reactors [32] [17] coupling thermohydraulics, thermomechanics, thermochemistry, thermodynamics, neutronics phenomena with characteristic time, length and mass going from microseconds to days, millimeters to meters, kilograms to hundred of tons. In shuch a context, this requires the simulation of the whole accident scenario or just a part of it leading to coupled problems of different size. Furthermore, simulation can be used for statistical analysis, e.g. Monte-Carlo sensitivity analysis, involving a large number of calculations, or simply to have a finer and better understanding of some phenomenons. Altogether and because of the lack of full physical and phenomenological knowledge, a wide range of models for the underlying physical phenomena are used, e.g. stationary models, reduced models, mesh based models, etc. In particular, **lumped parameter models** (LP models), sometimes called "0D" models, simplifie spatially distributed systems into discrete entities, e.g. partial differential equations become parameterized ordinary differential equations over time, in such a way that calculations require much less running time and a much lower computational cost. However, such simplifications come with a price to pay:

- LP models ignore the finite time of propagation of information of the continuous or space and time discretized model and instantly communicate and spread them;

- closure laws used in LP models are often described with highly non-linear functions of time and of the model internal state variables, e.g. correlations fitted from mesh based calculations or experimental results [3] [34];

- state, phase or topological changes in the continuous time and space model, e.g. disappearance, vaporization, are turned into instant internal changes and sometimes discontinuous event triggered at a certain time by the LP model, which can be compared to event occuring in *Differential Algebraic Equations* (DAE) [24]. A state change event missed by the simulation engine can bring the coupled models in a non coherent and non physical state during a small window of time resulting in numerical errors, numerical instabilities which have to be avoided at all cost;

As a result, coupled problems of LP models can have fast and stiff transients which are numerically challenging to solve.

There are two approaches to solve such coupled problems : a **monolithic** approach which solves the governing equations describing each model simultaneously and a **partitioned** approach [12], its counterpart, in which coupled models are associated to the so-called *partitions* which are solved one at a time during the coupling iterations. One of the advantage of such

partitioned approaches is that the solution of partitions can be done with different solvers adapted to the physical phenomenon involved in the partition. Moreover, great modularity and software reuse is achieved since partition solvers are assumed to be seen as "black box" by the partitioned problem with a set of inputs, a set of outputs and very limited internal details (e.g. derivative data) and thus can be easily exchanged. In this approach, partitions deliver physical quantities such as heat fluxes, forces, pressures, mass flow rates to other coupled partitions. In contrast with the monolithic approach, coupling equations between partitions are not part of a one block system of equations, instead, partitions are sharing data with external coupling equations corresponding to equilibrium conditions, e.g. heat flux equality between two thermal partitions sharing a geometrical interface [15] or temperature equality between a thermal partition and a thermodynamic partition sharing a common temperature. Because of possible decoupling effects between partitions, equilibrium conditions might not be enforced by the coupling algorithm leading to loosely or weakly coupled partitions. Therefore, there are two main classes of coupling schemes :

- **Explicit coupling schemes** (ECSs) [12, 8, 16, 11, 10, 9] which require only one call of each solver one after the other during each time step but which can only achieve weak coupling between the coupled partitions at the end of the time step.

- **Implicit coupling schemes** (ICSs) [18, 26, 14, 5, 19, 33, 6, 27, 13, 20] which require several calls of solvers within an iterative loop until a certain convergence threshold. If the scheme has converged, equations and subdomains are strongly coupled at the end of the time step, up to a certain precision, and the monolithic scheme is recovered.

In this paper, we focus on the numerical solution of heterogeneous 0D and 1D models by partitioned approaches. In this very specific context of modeling, we show how ECSs are often not suitable for the solution of such problems and implicit treatment is often necessary. We furthermore explain how regular ICSs are modified in order to take into account state change events triggered by the models. By this way, the coupled models can be synchronized on potential events and discontinuities.

The paper is structured as follows. Section 2 gives a brief overview of the lumped parameter mass and energy conservation governing equations in each subdomain and models used for the different previously cited phenomena ; for the sake of simplicity and conciseness, we only consider coupled thermalhydraulic phenomena. We believe that the extension to any other phenomena (e.g. thermochemistry, thermomechanic, neutronic, etc.) is similar. From there, the coupled formulation is explained and the
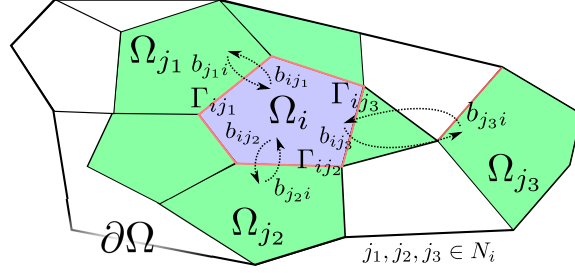
3

Figure 1: The abstract representation of domain decomposition of Ω focused on domain Ω_i and its neighbourhood $\Omega_{j \in N_i}$.

coupling algorithms are given in section 3. In section 4, we give numerical analysis, computations and discussions of a coupled problem solved with various coupling schemes within the PROCOR platform [21]. Finally, conclusion and opening remarks are given in section 5.

2 Governing equations

To simplify, we assume that the coupled problem to solve consists of different physics located at different subdomains. Figure 1 depicts a non overlapping domain decomposition of domain $\Omega = \cup_{i \in [\![1,m]\!]} \Omega_i$. Neighbouring domains Ω_j coupled with domain Ω_i communicating through interface Γ_{ij} can be actual geometrical neighbor of domain Ω_i, i.e. $\Gamma_{ij} = \partial\Omega_i \cap \partial\Omega_j \neq \emptyset$ or can be distant neighbor of domain Ω_i with whom it has linked but distant phenomena, i.e. $\partial\Omega_i \cap \partial\Omega_j = \emptyset$ and Γ_{ij} is a part of frontier $\partial\Omega_i$ of domain Ω_i. Neighbors of domain Ω_i are represented by the set $N_i = \{j \ / \ \exists \ \Gamma_{ij}\}$, with cardinality denoted by $n_i = \text{card}(N_i)$. Finally, frontier of domain Ω_i can be calculated by $\partial\Omega_i = \Gamma_i \cup (\cup_{j \in N_i} \Gamma_{ij})$. Subdomain Ω_i is described in terms of mass denoted by m_i [kg] and average temperature denoted by T_i [K]. We have :

$$m_i = \frac{1}{V_{\Omega_i}} \int_{\Omega_i} \rho \, dV, \quad T_i = \frac{1}{V_{\Omega_i}} \int_{\Omega_i} T \, dV.$$

The vector of state variables of subdomain Ω_i is denoted by $\mathbf{u}_i = (m_i, T_i)^{\text{t}}$. Note that in this article we decide to represent each subdomain in term of average temperature even though they could be represented in term of average enthalpy.

Interface variables are heat fluxes ϕ_{ij} [W.m^{-2}], temperature T_{ij} [K], mass flow rate $\dot{m}_{ij}$ [kg.s^{-1}] or surface area S_{ij} [m^2]. These variables are gathered in vector $\mathbf{b} = \{(\phi_{ij}, T_{ij}, \dot{m}_{ij}, S_{ij})^{\text{t}}\}$ for $i \in [1, m]$ and $j \in N_i$. The interface projector $\mathcal{P}_{ij}$ allows us to get interface Γ_{ij} vector variables $\mathbf{b}_{ij} = (\phi_{ij}, T_{ij}, \dot{m}_{ij}, S_{ij})^{\text{t}}$

4

from vector $\mathbf{b}$ with $\mathcal{P}_{ij}\mathbf{b} = \mathbf{b}_{ij}$.

We first describe the lumped parameter governing equations for each subdomain in section 2.1 and then present the interface equations between subdomains in section 2.2.

2.1 Subdomain lumped parameter equations

Subdomain Ω_i equations are expressed in terms of mass and energy macroscopic conservation equations (momentum conservation equations are modeled by closure laws, e.g. correlations for heat transfer coefficient). They are obtained from the local conservation equations, here Navier-Stokes equations under the Boussinesq approximation for liquid domains and heat equations for solid domains, integrated over the corresponding subdomain (see [22]). Tightly linked to the local physical model, this approach leads to the so-called LP model or "0D" model of the subdomain described by the two ordinary differential equations (ODE)

$$\frac{\mathrm{d}m_i}{\mathrm{d}t} = \sum_{j \in N_i} \dot{m}_{ij} \quad \text{in } \Omega_i, \tag{1}$$

$$m_i C p_i \frac{\mathrm{d}T_i}{\mathrm{d}t} + \sum_{j \in N_i} \dot{m}_{ij} C p_i (T_i - T_{ij}) = \sigma_i \phi_i S_i + \sum_{j \in N_i} \sigma_{ij} \phi_{ij} S_{ij} + m_i \dot{q}_i \quad \text{in } \Omega_i \tag{2}$$

with m_i [kg] the mass and T_i [K] the average temperature of Ω_i, ϕ_i [W.m^{-2}] the heating ($\sigma_i = 1$) or cooling ($\sigma_i = -1$) heat flux through boundary $\Gamma_i = \partial\Omega \cap \partial\Omega_i$ with temperature T_{b_i} and area S_i [m^2], ϕ_{ij} the heating or cooling heat flux and $\dot{m}_{ij}$ [kg.s^{-1}] the algebraic mass flow rate through Γ_{ij} with temperature T_{ij} and area S_{ij}. Finally, $C p_i$ [J.kg^{-1}.K^{-1}] is the heat capacity and $\dot{q}_i$ [W.kg^{-1}] is the residual power per mass unit coming from fission products of subdomain Ω_i.

The previous physical parameters are obtained from closure laws described hereafter in section 2.2. In particular, geometry dependent values, i.e. the characteristic length of a domain or the surface of an interface or the volume of a domain, are given by algebraic geometry equations. They take the form of algebraic functions, e.g. for the previous surface :

$$S_{ij} = S_{ij}(\rho_i, e_i, V_i) \tag{3}$$

with e_i [m] the characteristic length and V_i [m^3] the volume of domain Ω_i. Altogether, ordinary differential eqs. (1) and (2) combined with expressions like eq. (3) can be considered as *Differential Algebraic Equations* (DAE's) [28] describing the LP model.

2.2 Interface equations

In the present article, interfaces between two subdomains Ω_i and Ω_j can be of two types : free moving or fixed boundaries. Physically moving boundaries are, for example, boundaries between a liquid and a solid domain exchanging melted or solid materials. They are associated with a plane fusion solidification front corresponding to the Stefan condition at the interface (see [22] for further details). Fixed interfaces correspond to thermal equilibrium assuming no mass exchange through the interface and thermal conduction.

In case of a mobile interface, equilibrium conditions at the interface Γ_{ij} are given by

$$\dot{m}_{ij} = -\dot{m}_{ji} \quad \text{in } \Gamma_{ij}, \tag{4}$$

$$\phi_{ij}S_{ij} = -\phi_{ji}S_{ji} + \Delta\mathcal{H}^{\text{fus.}}\dot{m}_{ij} \quad \text{in } \Gamma_{ij}, \tag{5}$$

$$T_{ij} = T_{ji} = T^{\text{fus.}} \quad \text{in } \Gamma_{ij} \tag{6}$$

with $\Delta\mathcal{H}^{\text{fus.}}$ the fusion enthalpy and $T^{\text{fus.}}$ the fusion temperature of domain Ω_i, both assumed to be fixed. In particular, those conditions stipulate that the mass flow rate should be the same on both sides of the interface for mass conservation and that the heat fluxes should respect the Stefan condition. To simplify subdomain materials are treated as pure body and no thermochemistry is considered.

In case of a fixed interface, the thermal equilibrium conditions at interface Γ_{ij} are given by

$$\dot{m}_{ij} = -\dot{m}_{ji} = 0 \quad \text{in } \Gamma_{ij}, \tag{7}$$

$$T_{ij} = T_{ji} \quad \text{in } \Gamma_{ij}, \tag{8}$$

$$\phi_{ij}S_{ij} = -\phi_{ji}S_{ji} \quad \text{in } \Gamma_{ij} \tag{9}$$

Obviously, with the previous equations, appropriate closure laws for interface heat fluxes and temperatures are required. In traditional mesh based models, interface variables are given by a projection operator which are coherent with the domain equations, e.g. the restriction of the variables values over all the domain Ω_i to its interface $\Gamma_{ij} = \partial\Omega_i \cap \partial\Omega_j$, and thus are consistent with the physical equations. For LP models, interface variable $\mathbf{b}_{ij}$ is calculated from spatially averaged data $\mathbf{u}_i$ from domain Ω_i and data $(\{\mathbf{b}_{ij}\}_{j\in N_i}) \overset{\text{def}}{=} \mathbf{b}_{i\star}$ from the interfaces. They are given by closure laws which take the form of algebraic functions $\mathbf{b}_{ij} = \mathbf{b}_{ij}(\mathbf{u}_i, \mathbf{b}_{i\star})$. Thus they propagate data instantly, from one specific interface to all the other ones.

If the domain Ω_i is solid, such closure law functions for heat fluxes $\phi_{i\bullet}$ can be calculated from the heat diffusion conduction equation under

6

certain assumptions and approximations. A comparison of those different approximate models with a reference solution given by a finite element discretization of the heat conduction equation can be found in [22]. For example, the *stationary* model uses a 1D cylindrical with adiabatic lateral boundaries approximation and assumes a quadratic temperature profile in the solid domain. Conduction heat fluxes at interfaces Γ_{ij} and Γ_{ik} associated with the upper and lower cylinder surfaces are then given by the temperature derivative w.r.t the spatial direction leading to the closure law functions [22] :

$$\phi_{ij} = \phi_{ij}(\mathbf{u}_i, \mathbf{b}_{ik}) = \lambda_i \frac{6T_i - 4T_{ij} - 2T_{ik}}{e_i}, \tag{10}$$

$$\phi_{ik} = \phi_{ik}(\mathbf{u}_i, \mathbf{b}_{ij}) = \lambda_i \frac{6T_i - 4T_{ik} - 2T_{ij}}{e_i}. \tag{11}$$

Note, for instance, the instant propagation of interface Γ_{ik} temperature T_{ik} to interface Γ_{ij} in eq. (10) indicating that the *stationary* model gives closure law functions which propagate boundary related data **instantly** between interfaces of the domain.

Let us mention that, in the literature, one can find other nonlinear closure laws like $\phi_{ij}(\mathbf{u}_i, \mathbf{b}_{i\star}) \propto e_i^\alpha (T_i - T_{ij})^\beta$ with $\alpha, \beta \in \mathbb{R}$ for convective heat transfer or $\phi_{ij}(\mathbf{u}_i, \mathbf{b}_{i\star}) \propto T_{ij}^4$ for radiative heat transfer. In this paper, we will only consider eqs. (10) and (11).

3 Coupling formulation and schemes

3.1 Discretized coupling formulation and coupled problem

LP conservation equations eqs. (1) and (2) are then discretized in time at a lower level with a method of choice (e.g. explicit, implicit, Euler, Runge-Kutta, multistep methods, etc.) and then coupled in time on a higher level resulting in a two-level time scheme. At the highest level, those discretized equations are solved and coupled between times $t^0, t^1, \ldots, t^n, \ldots$ with a macro time step Δt and synchronized at each of these times. At the lowest level, each subdomain manages its own time integration scheme, its own micro time step δt and its own internal time. The integration scheme used by the subdomain is assumed to be adapted to the physical local problem. In the following, discretized values evaluated at time t^n are denoted by the superscript n.

We adopt the following notations. For each coupled subdomain $\{\Omega_i\}_{i \in [1,m]}$, discretized equations are represented by a function $\mathcal{F}_i^{\Delta t}$ used to solve and advance in time the problem of one time step Δt. This function takes as parameters the state vector $\mathbf{u}_i$ and the input interface variables $\{\mathbf{b}_{ji}\}_{j \in N_i} \overset{\text{def.}}{=} \mathbf{b}_{\star i}$

of domain Ω_i. Equations of the coupled problem are then given by

$$
\begin{cases}
\mathcal{F}_1^{\Delta t}(\mathbf{u_1}, \{\mathbf{b}_{j1}(\mathbf{u}_j, \mathbf{b}_{\star j})\}_{j \in N_1}) = 0 \\
\mathcal{F}_2^{\Delta t}(\mathbf{u_2}, \{\mathbf{b}_{j2}(\mathbf{u}_j, \mathbf{b}_{\star j})\}_{j \in N_2}) = 0 \\
\qquad \vdots \\
\mathcal{F}_m^{\Delta t}(\mathbf{u_m}, \{\mathbf{b}_{jm}(\mathbf{u}_j, \mathbf{b}_{\star j})\}_{j \in N_m}) = 0
\end{cases}
\tag{12}
$$

in such a way that the inter dependencies between domain Ω_i and its neighbors are highlighted by the closure law functions $\{\mathbf{b}_{ji}\}_{j \in N_i}$ which is function of the coupled subdomain internal variable $\mathbf{u}_j$ and interface variables $\mathbf{b}_{\star j}$, which might in turn need values from domain Ω_i to be calculated.

Those interface dependencies highlight the input-output relationship between interface variables of the different subdomains. This suggests that solvers can be seen as closed entities or "black-boxes" taking input interface variables $\mathbf{b}_{\star i}$ from neighboring subdomains and giving back output interface variables $\mathbf{b}_{i\star}$ to neighboring subdomains. Therefore, it seems natural to represent solver of domain Ω_i as a function $\mathcal{M}_i^{\Delta t} : \mathbb{R}^{3 \times n_i} \mapsto \mathbb{R}^{3 \times n_i}$ in which we explicitly hide subdomain state variable $\mathbf{u}_i$ and its integration, and only the input and output interface variables are visible. It is possible that we have access to limited information about them, e.g. no derivative data. For instance, solver of domain Ω_i is defined by

$$
\mathbf{b}_{i\star} = \mathcal{M}_i^{\Delta t}(\mathbf{b}_{\star i}).
\tag{13}
$$

From eq. (13), we can define the coupled problem at interface Γ_{ij} in term of solvers :

$$
\mathbf{b}_{ij} = \mathcal{P}_{ij} \circ \mathcal{M}_i^{\Delta t} \left(\mathbf{b}_{ji}, \{\mathbf{b}_{ki}\}_{k \in N_i, \, k \neq j} \right),
\tag{14}
$$

$$
\mathbf{b}_{ji} = \mathcal{P}_{ji} \circ \mathcal{M}_j^{\Delta t} \left(\mathbf{b}_{ij}, \{\mathbf{b}_{kj}\}_{k \in N_j, \, k \neq i} \right)
\tag{15}
$$

with $\mathcal{P}_{ij}$ the interface Γ_{ij} projector. Those equations emphasize the "action-reaction" at interface between the two domains : a slight modification of interface variable $\mathbf{b}_{ji}$ will in turn change the associated interface variable $\mathbf{b}_{ij}$, and vice versa. The strength of the associated coupling is represented by the Jacobian matrices $\{\frac{\partial \mathcal{M}_i^{\Delta t}}{\partial \mathbf{b}_{ki}}\}_{k \in N_i}$ and $\{\frac{\partial \mathcal{M}_j^{\Delta t}}{\partial \mathbf{b}_{kj}}\}_{k \in N_j}$. Moreover it is difficult to evaluate this strength since they may not be available.

Combining eq. (14) with eq. (15) gives the widely used fixed point equation at interface Γ_{ij} (see [25])

$$
\mathbf{b}_{ij} = \mathcal{P}_{ij} \circ \mathcal{M}_i^{\Delta t} \left(\mathcal{P}_{ji} \circ \mathcal{M}_j^{\Delta t} \left(\mathbf{b}_{ij}, \{\mathbf{b}_{kj}\}_{k \in N_j, \, k \neq i} \right), \{\mathbf{b}_{ki}\}_{k \in N_i, \, k \neq j} \right)
\tag{16}
$$

which allows us to define the residual operator $\mathcal{R}_{ij}$ at interface Γ_{ij} by

$$\mathcal{R}_{ij}(\mathbf{b}_{ij}) \overset{def}{=} \mathcal{P}_{ij} \circ \mathcal{M}_i^{\Delta t} \left(\mathcal{P}_{ji} \circ \mathcal{M}_j^{\Delta t} \left(\mathbf{b}_{ij}, \{\mathbf{b}_{kj}\}_{k \in N_j,\ k \neq i} \right), \{\mathbf{b}_{ki}\}_{k \in N_i,\ k \neq j} \right) - \mathbf{b}_{ij}$$
(17)

for a guess candidate $\mathbf{b}_{ij}$. The residual $\mathcal{R}_{ij}(\mathbf{b}_{ij})$ will express the imbalance created at interface Γ_{ij} : if domains Ω_i and Ω_j are strongly coupled, equilibrium conditions at interface are fulfilled and the interface residual is null, otherwise the two domains are only weakly coupled.

3.2 Coupling schemes

Explicit coupling schemes (ECSs). Referred to as "conventional serial staggered" in [12], ECSs solve the coupled problem with one call of solver per time step. They are based on a Gauss-Seidel semi-explicit solution of the coupled problem eq. (12). Obviously, another scheme based on a fully-explicit or Jacobi solution can be used to allow for more algorithm parallelism. If we assume that solver $\mathcal{M}_i^{\Delta t}$ is solved before solver $\mathcal{M}_j^{\Delta t}$, the scheme solves at interface Γ_{ij} :

$$\mathbf{b}_{ij}^{n+1} = \mathcal{P}_{ij} \circ \mathcal{M}_i^{\Delta t} \left(\mathbf{b}_{ji}^n, \{\mathbf{b}_{ki}^\bullet\}_{k \in N_i,\ k \neq j} \right),$$
(18)

$$\mathbf{b}_{ji}^{n+1} = \mathcal{P}_{ji} \circ \mathcal{M}_j^{\Delta t} \left(\mathbf{b}_{ij}^{n+1}, \{\mathbf{b}_{kj}^\bullet\}_{k \in N_j,\ k \neq i} \right)$$
(19)

with $\mathbf{b}_{ki}^\bullet$ is evaluated at t^n or t^{n+1} if solver $\mathcal{M}_k^{\Delta t}$ is called before or after solver $\mathcal{M}_i^{\Delta t}$.

While potentially attractive and fast since only one call per solver is done during each time step, it is well known that this scheme yields poor accuracy and stability issues [30]. Because of the *time-lag* caused by the semi-explicit resolution, it is unlikely that interface residuals defined by eq. (17) are null and equilibrium conditions are not enforced at interface. Besides, despite several improvements and studies in [8] [16] [11] [10] [9] [29], the weak coupling reached by explicit coupling schemes is often not enough and only a strong coupling at the end of the time step can ensure proper stability properties [4] [15].

Implicit coupling schemes (ICSs). A way to fix the *time-lag* is to use implicit coupling between subdomains. At interface Γ_{ij}, implicit coupling gives :

$$\mathbf{b}_{ij}^{n+1} = \mathcal{P}_{ij} \circ \mathcal{M}_i^{\Delta t} \left(\mathbf{b}_{ji}^{n+1}, \{\mathbf{b}_{ki}^{n+1}\}_{k \in N_i,\ k \neq j} \right),$$
(20)

$$\mathbf{b}_{ji}^{n+1} = \mathcal{P}_{ji} \circ \mathcal{M}_j^{\Delta t} \left(\mathbf{b}_{ij}^{n+1}, \{\mathbf{b}_{kj}^{n+1}\}_{k \in N_j,\ k \neq i} \right)$$
(21)

We clearly see that eqs. (20) and (21) give discrete interface values respecting the fixed point eq. (16) leading to a null interface residual. Hence, interface Γ_{ij} is at equilibrium and a strong coupling between equations is obtained. However, while being mathematically interesting, eqs. (20) and (21) do not allow to decouple the two equations at each time step and it is often more convenient to use iterative methods to solve them. By iterative methods we mean methods using iterative processes inside one coupling iteration, i.e. between times t^n and t^{n+1}, until a convergence criterion is reached. In that case interface variables *verify* (with an error bounded by the convergence criterion) at each interface the associated fixed point eq. (16) leading to a strong coupling between equations of the coupled problem. At interface Γ_{ij} between domain Ω_i and Ω_j, the block Gauss-Seidel coupling scheme, also known as staggered or partitioned coupling scheme, is an iterative method based on Newton-Raphson iterations of the fixed point eq. (16) given by

$$\mathbf{b}_{ji}^{n+1,k+1} = \mathbf{b}_{ji}^{n+1,k} + \left(\frac{\mathrm{d}\mathcal{R}_{ji}}{\mathrm{d}\mathbf{b}_{ji}} \Big|_{\mathbf{b}_{ji}^{n+1,k}} \right)^{-1} (-\mathcal{R}_{ji}(\mathbf{b}_{ji}^{n+1,k})) \tag{22}$$

with the residual $\mathcal{R}_{ji}(\mathbf{b}_{ji}^{n+1,k})$ at iteration k defined by

$$\mathcal{R}_{ji}(\mathbf{b}_{ji}^{n+1,k}) = \mathbf{r}_{ji}^{n+1,k} = \mathcal{M}_j^{\Delta t} \circ \mathcal{M}_i^{\Delta t}(\mathbf{b}_{ji}^{n+1,k}) - \mathbf{b}_{ji}^{n+1,k} \tag{23}$$

which allows us to define a convergence criterion for the iterative process by

$$\frac{\left\| \mathcal{M}_j^{\Delta t} \circ \mathcal{M}_i^{\Delta t}(\mathbf{b}_{ji}^{n+1,k}) - \mathbf{b}_{ji}^{n+1,k} \right\|}{\left\| \mathbf{b}_{ji}^{n+1,k} \right\|} = \frac{\left\| \mathbf{r}_{ji}^{n+1,k} \right\|}{\left\| \mathbf{b}_{ji}^{n+1,k} \right\|} \leq \epsilon_{\mathrm{rel}} \tag{24}$$

with ϵ_{rel} the relative stopping criterion for the subiterative process. *Gauss-Seidel* or *staggered* symbolizes the way interfaces data are sequenced through solvers (or *block*) inside coupling iterations.

Remark on Jacobian matrices and associated solvers. In eq. (22), the Jacobian matrix or its inverse are usually not known and/or not calculable since solvers are seen as black-box solvers, thus the iterations can only be approximated by approximation of the Jacobian matrix or its inverse leading to Quasi-Newton techniques. In [14], Gerbeau and al. use reduced order models to calculate the Jacobian matrix. In [26], Michlet and al. use Newton-Krylov subiterations to approximate the Jacobian matrix leading to the so-called *Jacobian free Newton-Krylov* method. From previous residuals, Degroote and al. in [5] solve least-squares problems to approximate the inverse of the Jacobian matrix leading to *Interface Quasi-Newton - Inverse*

Least-Squares (IQN-ILS) methods while Vierendeels and al. [33] approximate the Jacobian matrix with similar methods leading to *Interface Quasi-Newton - Least-Squares* (IQN-LS). Multigrid Quasi-Newton methods are also studied in [6]. A recent review of different Quasi-Newton methods can be found in [27] for fluid-structure interaction and in [13] for thermal-structure interaction.

Much cheaper methods use relaxation techniques for the interface variable iterations which consists in using an approximation of the inverse of the interface residual Jacobian matrix of the form

$$\left(\frac{\mathrm{d}\mathcal{R}_{ji}}{\mathrm{d}\mathbf{b}_{ji}}\bigg|_{\mathbf{b}_{ji}^{n+1,k}}\right)^{-1} \approx -\omega^k I \tag{25}$$

for which the fixed point iterations with dynamic relaxation are given by

$$\mathbf{b}_{ji}^{n+1,k+1} = \omega^k \mathcal{M}_j^{\Delta t} \circ \mathcal{M}_i^{\Delta t}(\mathbf{b}_{ji}^{n+1,k}) + (1 - \omega^k)\mathbf{b}_{ji}^{n+1,k}. \tag{26}$$

Note that for $\omega^k = 1$, iterations given by eq. (26) are classical Picard iterations which converge generally only linearly and very slowly. In [20], the authors show that the block Gauss-Seidel iterative method with relaxation techniques for the resolution of equation eq. (22) can be very efficient at a surprisingly low cost in comparison to more elaborated Quasi-Newton methods. Besides, it is shown in [31] that these techniques are also proven to be very competitive in comparison to the direct solution of the nonlinear problem given by eq. (22) with traditional Newton-Raphson methods using derivative data. In this paper, we focus on block Gauss-Seidel iterative method with relaxation techniques.

For instance, the solution of equation eq. (22) by the Steffensen's method accelerated with Aitken's delta-squared Δ^2 method [1] can be cast into fixed point iterations with dynamic relaxation leading to methods of order 2, see [31]. Less costly but with a convergence rate of the golden ratio $\frac{1+\sqrt{5}}{2}$, the fixed point iterations given by the secant method can also be seen as fixed point iterations with dynamic relaxation leading to

$$\omega^k = -\omega^{k-1} \frac{\langle \mathbf{r}_{ji}^{n+1,k} - \mathbf{r}_{ji}^{n+1,k-1}, \mathbf{r}_{ji}^{n+1,k-1} \rangle}{\langle \mathbf{r}_{ji}^{n+1,k} - \mathbf{r}_{ji}^{n+1,k-1}, \mathbf{r}_{ji}^{n+1,k} - \mathbf{r}_{ji}^{n+1,k-1} \rangle}. \tag{27}$$

One can also use constant relaxation given by a constant parameter ω. However, this requires the determination of the best relaxation parameters, i.e. leading to the highest rates of convergence, which is highly problem-dependent.
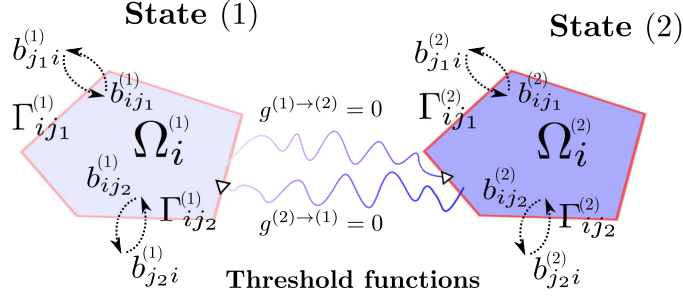
Figure 2: The abstract representation of states $\Omega_i^{(1)}$ and $\Omega_i^{(2)}$ of domain Ω_i. Each state has its own interfaces $\Gamma_\bullet^{(1)}$ and $\Gamma_\bullet^{(2)}$ with associated variables $\mathbf{b}_\bullet^{(1)}$ and $\mathbf{b}_\bullet^{(2)}$. A state transition occurs when a transition function crosses zero.

Implicit coupling schemes for event detection and model synchronization. In LP modeling, state transitions are triggered by internal events corresponding to activation of threshold functions. This activation is dependent on input from the coupled models and thus times of events are unknowns of the coupled problem. As depicted fig. 2, each state has its own solver, its own set of equations and its own interface and boundary conditions.

State transition can lead to discontinuities of state or interface variables. A missed event can lead to inconsistent and incoherent physical states, e.g. the disappearance of a model not seen by other coupled models, and/or mathematical difficulties with non-smooth functions in the coupled problem eq. (12) bringing usual theorems out of their scope of validity, with possibly breakdown issue like divergence of Newton iterations.

During one coupling time step Δt, the coupling scheme must be able to adapt its time step to synchronize all the models on the time of the first event. However, synchronization strategies are hard to achieve with ECSs which can often only synchronized coupled models at each coupled time step leading to time detection errors of order $O(\Delta t)$. Hereafter, we describe how the previous ICSs can be used for event detection to ensure proper synchronization between models.

Let us consider the coupling at interface Γ_{ij} between domain i and j. As depicted in fig. 3, internal events are triggered during one coupling time step Δt by solver $\mathcal{M}_i$ and/or solver $\mathcal{M}_j$ at respective times $t_i^\star$ and $t_j^\star$ between t^n and $t^n + \Delta t$. When an event occurs, the solver stops its computation and do not compute the whole coupling time step Δt. Solvers should be synchronized on the first triggered event at time $t^\star = t_j^\star$.

During a fixed point iteration of an ICS starting at time t^n and ending at the previously calculated time of first event $t^{\star,k}$, events are trigerred at times $t_i^{\star,k}$ and $t_j^{\star,k}$ by solvers. The aim is to build an iterative algorithm calculating

12

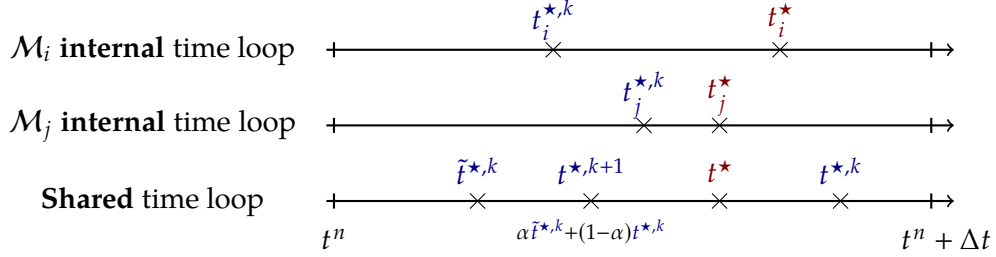Figure 3: Shared coupling time loop and internal time loops of solvers $\mathcal{M}_i$ and $\mathcal{M}_j$. Internal events at times $t_i^\star$ and $t_j^\star$ are to be detected by the scheme in order to synchronize on time $t^\star$ of the first event. An ICS detects event at times $t_i^{\star,k}$ and $t_j^{\star,k}$ and has to calculate the new iteration $t^{\star,k+1}$ in such a way that $t^{\star,\infty} \approx t^\star$.

the new iteration $t^{\star,k+1}$ in such a way that : $t^{\star,\infty} \approx t^\star$. Algorithm 1 gives a sequence to calculate this new iteration. At convergence, the coupled problem has been solved between times t^n and $t^{n+1} = t^{\star,\infty}$. The next coupling time step then starts at time t^{n+1} with the same algorithm.

Concluding remarks regarding the designed iterative algorithm. At convergence $k = \infty$ of a coupling time step between times t^n and t^{n+1} at interface Γ_{ij}, we get that :

- Model i and model j are strongly coupled because the fixed point eq. (16) is verified with at most an error bounded by the tolerance ϵ_{rel} of the scheme, i.e.

$$\frac{\left\| \mathcal{M}_j^{\Delta t} \circ \mathcal{M}_i^{\Delta t}(\mathbf{b}_{ji}^{n+1,\infty}) - \mathbf{b}_{ji}^{n+1,\infty} \right\|}{\left\| \mathbf{b}_{ji}^{n+1,\infty} \right\|} \leq \epsilon_{\text{rel}}.$$

- Model i and model j are synchronized on potential internal triggered events. In particular, they are synchronized on the time of the first event with an error also bounded by the tolerance ϵ_{rel}, i.e.

$$\frac{\left| t^{n+1} - t^\star \right|}{\Delta t} = \frac{\left| t^{\star,\infty} - t^\star \right|}{\Delta t} \leq \epsilon_{\text{rel}}$$

4 Numerical analysis and examples

In the following, the aim is to present numerical solutions of some coupled LP models implemented in the CEA's PROCOR platform with both ECSs and ICSs. The industrial PROCOR platform [21] allows generic "black-box"

13

Algorithm 1 Calculate the new iteration $t^{\star,k+1}$

1: Compute a new fixed point iteration between solvers $\mathcal{M}_i^{\Delta t}$ and $\mathcal{M}_j^{\Delta t}$ with an ICS;
2: **if** *an event has occurred for model $l \in \{i,j\}$* **then**
3:     $t_l^{\star,k} \leftarrow$ the corresponding event time;
4: **else**
5:     $t_l^{\star,k} \leftarrow t^n + \Delta t$;
6:     /* the whole coupling time step Δt was computed. */
7: **end if**
8: $\tilde{t}^{\star,k} \leftarrow \min(t_i^{\star,k}, t_j^{\star,k})$;
9: **if** $(|\tilde{t}^{\star,k} - t^{\star,k}|/\Delta t < \epsilon_{\text{rel}})$ **and** (*the ICS has converged at interface Γ_{ij}*) **then**
    /* ϵ_{rel} being a tolerance given by the ICS. */
10:     $t^{\star,k+1} \leftarrow \tilde{t}^{\star,k}$;
11:     $t^{\star,\infty} \leftarrow t^{\star,k+1}$;
12: **else**
13:     $t^{\star,k+1} \leftarrow \alpha \tilde{t}^{\star,k} + (1 - \alpha)t^{\star,k}$;
14:     /* $\alpha \in]0,1[$ being a relaxation parameter given by the ICS. */
15: **end if**

---

physical models coupling solved by various ECSs and ICSs. It is dedicated to the fast robust setup of coupled problems taking the form of complex systems [2] for the simulation of severe accidents in nuclear reactors. For computational efficiency reasons in this industrial context, one important constraint is that we want to be able to keep a sufficiently large coupling time step in comparison to the characteristic times of the physical phenomena being involved. With this constraint, it will be shown that even "simple" coupled problems of LP models may produce unexpected artifacts in terms of coupling and synchronization and how the use of ICSs to solve them can provide benefits.

For instance, let us consider the heat conduction between domains Ω_1 and Ω_2 calculated respectively by solvers $\mathcal{M}_1$ and $\mathcal{M}_2$. As depicted in fig. 4, solvers are coupled at interface $\Gamma_{12} = \partial \Omega_1 \cap \partial \Omega_2$ of unit area $S = 1$ with Dirichlet-Neumann boundary conditions given by eqs. (4) to (6) or eqs. (7) to (9). This coupling ensure the well posedness of the domain decomposition problem [7]. For this coupled problem, two types of heat conduction solvers are used : LP solvers and finer solvers based on a space discretization of the 1D heat equation. Finally, we assume a cylindrical geometry in such a way that the length and mass of each domain are related with $m_{\{1,2\}} = \rho_{\{1,2\}} S e_{\{1,2\}} = \rho_{\{1,2\}} e_{\{1,2\}}$.
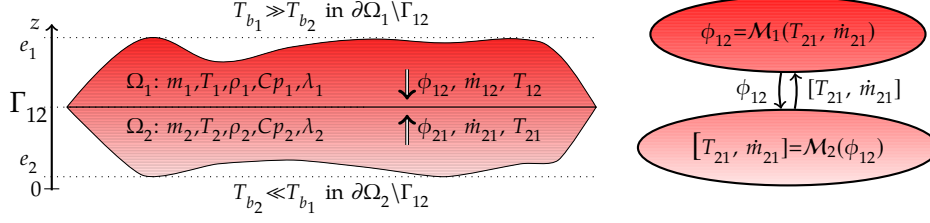
Figure 4: Heat conduction between domains Ω_1 and Ω_2 : notations (*left*) and Dirichlet-Neumann coupling of solvers $\mathcal{M}_1$ and $\mathcal{M}_2$ (*right*).

4.1 Linear stability of the coupling of lumped parameter solvers

First, we consider the Dirichlet-Neumann boundary conditions at the fixed interface Γ_{12} given by eqs. (7) to (9) $\dot{m}_{12} = -\dot{m}_{21} = 0, T_{12} = T_{21}, \phi_{12} = -\phi_{21}$. The two domain masses are constant and only their energy conservation equations are calculated. In the following, we analyze the linear stability of the coupling of LP solvers. They are based on a time discretization of the energy conservation eq. (2) and closure laws eqs. (10) and (11) to solve the heat conduction problem. A similar stability analysis for finer 1D solvers can be found in [15].

4.1.1 Stability of a *toy* explicit coupling scheme

The aim here is to build a prototype of a 'toy' ECS with no subcycling and only one level of time discretization. Such coupling scheme should allow us to solve the coupled problem while solvers of domains Ω_1 and Ω_2 are only called once during a time step. To do so, we use an implicit Euler scheme for the first domain Ω_1 and an explicit Euler scheme for the second domain Ω_2 . Denoting by Δt the time step, the discretized equations for the first domain Ω_1 are given by

$$
\begin{cases}
\phi_{12}^n = \lambda_1 \dfrac{6T_1^n - 2T_{b_1} - 4T_{12}^n}{e_1} & \text{in } \Omega_1 \\[2mm]
\rho_1 Cp_1 e_1 \dfrac{T_1^n - T_1^{n-1}}{\Delta t} = -\phi_{12}^n & \text{in } \Omega_1
\end{cases}
\tag{28}
$$

with continuity of temperature at the interface, i.e.

$$
T_{12}^n = T_{21}^n \quad \text{on } \Gamma_{12}
\tag{29}
$$

and for the second domain Ω_2

$$
\begin{cases}
T_{21}^{n+1} = -\dfrac{1}{4}\dfrac{e_2}{\lambda_2}\phi_{21}^n + \dfrac{3}{2}T_2^{n+1} - \dfrac{1}{2}T_{b_2} & \text{in } \Omega_2 \\[2mm]
\rho_2 Cp_2 e_2 \dfrac{T_2^{n+1} - T_2^n}{\Delta t} = -\phi_{21}^n & \text{in } \Omega_2
\end{cases}
\tag{30}
$$

15

with continuity of heat flux at the interface, i.e.

$$\phi_{21}^n = -\phi_{12}^n \quad \text{on } \Gamma_{12}. \tag{31}$$

The ECS is sequenced as follows : given an interface temperature T_{21}^n at time t^n, the first domain is advanced from time t^{n-1} to t^n and a heat flux ϕ_{12}^n is computed at time t^n which is then imposed to the second domain. It is then advanced from time t^n to t^{n+1} and it computes a new temperature T_{21}^{n+1} at time t^{n+1}, and so on. Thus, the coupling scheme only requires one call to each solver per time step so that the scheme can be called explicit.

We now analyze the linear stability of the coupling scheme. Combining eqs. (28) to (31), we get

$$\left(1 + 6\frac{\Delta t}{\tau_1}\right)\phi_{12}^{n+1} - \left(1 + \left(1 - 6\frac{\Delta t}{\tau_2}\right)\hbar\right)\phi_{12}^n + \hbar\,\phi_{12}^{n-1} = 0 \tag{32}$$

with $\hbar = \frac{\lambda_1/e_1}{\lambda_2/e_2}$, the characteristic times of conduction $\tau_1 = \rho_1 C_{p_1} e_1{}^2/\lambda_1$ in domain Ω_1 and $\tau_2 = \rho_2 C_{p_2} e_2{}^2/\lambda_2$ in domain Ω_2. To ensure stability of the explicit scheme in domain Ω_2, Δt has to be small in comparison to τ_2, i.e. $\Delta t/\tau_2 \ll 1$. The simplified characteristic polynomial χ associated to the simplified second order linear difference eq. (32) has two complex roots $x_{\{1,2\}}^\star$ which have to be of modulus strictly smaller than one in order to guaranty a stable coupling scheme.

We get the following results :

- When $\Delta t/\tau_1 \ll 1$ and $\hbar < 1$, the two roots are real and a Taylor expansion gives

$$x_1^\star = 1 - \frac{6}{1-\hbar}\frac{\Delta t}{\tau_1} + O\!\left(\left(\frac{\Delta t}{\tau_1}\right)^2\right)$$

$$x_2^\star = \hbar + \frac{6\hbar^2}{1-\hbar}\frac{\Delta t}{\tau_1} + O\!\left(\left(\frac{\Delta t}{\tau_1}\right)^2\right)$$

  When $\Delta t/\tau_1 \ll 1$ and $\hbar > 1$, the two roots are complex of modulus

$$\left|x_{\{1,2\}}^\star\right|^2 = \frac{\hbar}{1 + 6\frac{\Delta t}{\tau_1}}$$

- For any values of $\Delta t/\tau_1$, when $\hbar \ll 1$, roots of the characteristic polynomial χ are $x_1^\star \approx \frac{1}{1+6\frac{\Delta t}{\tau_1}}$ and $x_2^\star \approx \frac{\hbar}{1+6\frac{\Delta t}{\tau_1}}$ and when $\hbar \gg 1$, $x_1^\star \approx 1 + \frac{6\frac{\Delta t}{\tau_1}}{\hbar}$ and $x_2^\star \approx \frac{\hbar}{1+6\frac{\Delta t}{\tau_1}}$.

Thus, in both cases when $\hbar > 1$ the spurious solution for ϕ_{12} of eq. (32) associated to root $x_2^\star$ increases with a growth rate of $\frac{\hbar}{1+6\,\Delta t/\tau_1}$. In most cases, the spurious solution will grow in time leading to an unstable scheme. On the contrary, cases when $\hbar < 1$ give a stable coupling scheme.

Thus, the remaining question is the value $\hbar^{\mathrm{crit}}$ of $\hbar$ above which the instabilities appear, thus defining the stability limit region of the ECS. Further calculations show that $\hbar^{\mathrm{crit}} = \left|\frac{1+\,6\,\Delta t/\tau_1}{1-\,6\,\Delta t/\tau_2}\right|$ allowing to define a *pseudo* CFL condition for the linear stability of the ECS :

$$r_{12}(\Delta t) \stackrel{def.}{=} \left|\frac{1-\,6\,\Delta t/\tau_2}{1+\,6\,\Delta t/\tau_1}\right|\hbar < 1 \tag{33}$$

Finally, the Dirichlet-Neumann explicit coupling should be done in such a way that the domain with the Dirichlet boundary condition, i.e. imposed boundary temperature, has the lower thermal conductivity or the higher characteristic length and the domain with the Neumann boundary condition, i.e. imposed boundary heat flux, has the higher thermal conductivity and the lower characteristic length. Thus, the stability limit region $\hbar^{\mathrm{crit}}$ can be extended for larger values of $\Delta t/\tau_1$ which can be explained by the diffusive properties of the ICS used in domain Ω_1.

Numerical evidence of stability. This analysis is illustrated by fig. 5. At $t = 0^-$, both domains are at an equilibrium temperature of $T_1 = T_2 = T_{21} = T_{b_1} = T_{b_2} = 2000$ K. Boundary discontinuities are imposed at $t = 0^+$, $T_{b_1} = 3000$ K and $T_{b_2} = 400$ K and at $t = 3\,\tau_1$, $T_{b_1} = T_{b_2} = 2000$ K. In addition, all of the computations use the value $\Delta t/\tau_2 = 1/100$ and $\Delta t/\tau_1 = 1/10$ corresponding to a stability limit region $\hbar^{\mathrm{crit}} = 1.6$. Figure 5a shows that when $\hbar = \hbar^{\mathrm{crit}}$ the oscillations created by the transient initiated by the boundary discontinuities are not damped but are stable while in contrary in fig. 5c with $\hbar < \hbar^{\mathrm{crit}}$ the oscillations are well damped and in fig. 5d with $\hbar > \hbar^{\mathrm{crit}}$ the oscillations are clearly unstable. However, those three figures show that the discontinuities at boundaries are instantly propagated to the interface temperature and to the coupled domain in only one coupling time step. For comparison purpose, solution given by the coupling of the 1D heat equation solvers is given in fig. 5b. For the computation, the same physical values as for the coupling of LP solvers are used. The values meet the requirements expressed in [15] to ensure proper stability of such solvers. For this coupling, the discontinuities at boundaries start a much slower and smaller transient ($T_{21}(t = 1000\,\mathrm{s}) \approx 2150$ K) than for the LP coupling ($T_{21}(t = 100\,\mathrm{s}) \approx 2700$ K). The fact that LP models propagate in one coupling time step all their discontinuities to the other models tend to create fast and important transient. Thus, the use of ECS might not be adapted for this case.
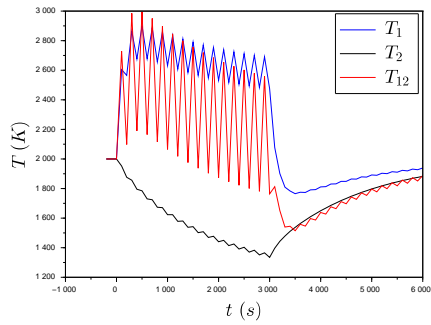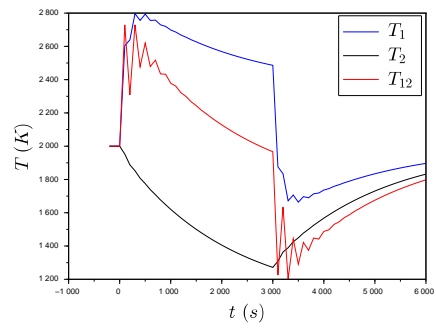
(a) LP solvers, $\hbar = 1.6$
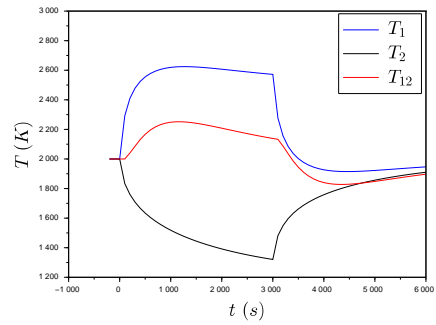
(b) multidimensional solvers, $\hbar = 1.6$

(c) $\hbar = 1.63$
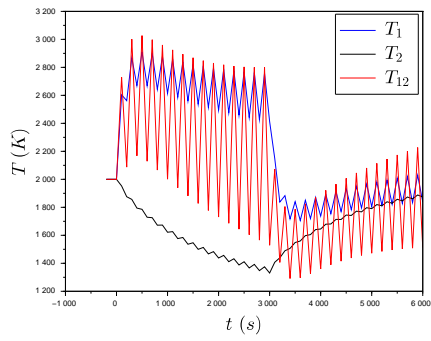
(d) $\hbar = 1.0$

Figure 5: Propagation of discontinuities at boundaries in the explicit coupling of lumper parameter and finer (upper right) solvers for heat conduction for different values of $\hbar$ with $\Delta t / \tau_2 = 1/100$ and $\Delta t / \tau_1 = 1/10$.

4.1.2 Stability of a *toy* implicit coupling scheme

The iterative algorithm is described below. Given an initial boundary temperature $T_{21}^{n+1,0}$ for domain Ω_1, it iterates over $k \geq 0$ with the following steps :

1. Use an **implicit** solver in Ω_1 to find the interface heat flux $\phi_{12}^{n+1,k+1}$

$$
\begin{cases}
\phi_{12}^{n+1,k+1} = \lambda_1 \dfrac{6T_1^{n+1} - 2T_{b_1} - 4T_{12}^{n+1}}{e_1} & \text{in } \Omega_1 \\[4mm]
\rho_1 C_{p_1} e_1 \dfrac{T_1^{n+1} - T_1^n}{\Delta t} = -\phi_{12}^{n+1,k+1} & \text{in } \Omega_1
\end{cases}
\tag{34}
$$

with continuity of temperature at the interface, i.e.

$$
T_{12}^{n+1} = T_{21}^{n+1,k} \quad \text{on } \Gamma_{12}.
\tag{35}
$$

2. Use an **implicit** solver in Ω_2 to find the interface temperature $\tilde{T}_{21}^{n+1,k+1}$

$$
\begin{cases}
\tilde{T}_{21}^{n+1,k+1} = -\dfrac{1}{4}\dfrac{e_2}{\lambda_2}\phi_{21}^{n+1} + \dfrac{3}{2}T_2^{n+1} - \dfrac{1}{2}T_{b_2} & \text{in } \Omega_2 \\[4mm]
\rho_2 C_{p_2} e_2 \dfrac{T_2^{n+1} - T_2^n}{\Delta t} = -\phi_{21}^{n+1} & \text{in } \Omega_2
\end{cases}
\tag{36}
$$

with continuity of heat flux at the interface, i.e.

$$
\phi_{21}^{n+1} = -\phi_{12}^{n+1,k+1} \quad \text{on } \Gamma_{12}.
\tag{37}
$$

3. Measure convergence level with

$$
\dfrac{\left| \tilde{T}_{21}^{n+1,k+1} - T_{21}^{n+1,k} \right|}{T_{21}^{n+1,k}} \leq \epsilon_{\text{rel}}.
\tag{38}
$$

If the previous predicate is not satisfied, relax the interface temperature by

$$
T_{21}^{n+1,k+1} = \omega \tilde{T}_{21}^{n+1,k+1} + (1 - \omega)T_{21}^{n+1,k}
\tag{39}
$$

and loop again. Otherwise, the final interface heat flux and temperature are given by $T_{21}^{n+1} = T_{21}^{n+1,k}$ and $\phi_{12}^{n+1} = \phi_{12}^{n+1,k}$. Consequently, internal variables T_1^{n+1} and T_2^{n+1} can be fully implicitly calculated : the iterative algorithm effectively allows to use implicit solvers for the two domains while allowing to decouple the two domains.

Combining eqs. (34) to (37), simple calculations lead to the following equation giving the interface temperature iterates $T_{21}^{n+1,k}$

$$T_{21}^{n+1,k+1} = \left[1 - \left(1 + \frac{1 - 6\frac{\Delta t}{\tau_2}}{1 + 6\frac{\Delta t}{\tau_1}}\hbar\right)\omega\right] T_{21}^{n+1,k} + g(T_1^n, T_2^n, T_{b_1}, T_{b_2}). \qquad (40)$$

We note T_{21}^{n+1} the solution of the fixed point equation associated with the previous equation and $e_k = \left| T_{21}^{n+1,k} - T_{21}^{n+1} \right|$ the error at iteration k. Then iteration errors are given by equation

$$e_{k+1} = \left| 1 - \left(1 + \frac{1 - 6\frac{\Delta t}{\tau_2}}{1 + 6\frac{\Delta t}{\tau_1}}\hbar\right)\omega\right| e_k. \qquad (41)$$

Thus, the iterative algorithm converges toward the interface solutions, i.e. $T_{21}^{n+1,\infty} = T_{21}^{n+1}$ and $\phi_{12}^{n+1,\infty} = \phi_{12}^{n+1}$, if and only if

$$0 < \omega < \frac{2}{1 + \left|\frac{1 - 6\frac{\Delta t}{\tau_2}}{1 + 6\frac{\Delta t}{\tau_1}}\right|\hbar} = \frac{2}{1 + r_{12}(\Delta t)}. \qquad (42)$$

Note that when $\frac{\Delta t}{\tau_1} \ll 1$ and $\frac{\Delta t}{\tau_2} \ll 1$, condition eq. (42) reads

$$0 < \omega < \frac{2}{1 + \hbar}. \qquad (43)$$

In cases where $\hbar > 1$ for which the ECS diverges, the iterative algorithm needs $\omega < 1$, i.e. under-relaxation to converge, which might lead to slow convergence.

Numerical evidence of stability. This analysis is confirmed by fig. 6. As in section 4.1.1, both domains are at an equilibrium temperature of 2000 K and the same discontinuities at boundaries are occurring at the same time $t = 0^+$ and $t = 3\tau_1$. For the computations, we still use $\Delta t/\tau_2 = 1/100$, $\Delta t/\tau_1 = 1/10$. We use $\hbar = 1.6$ corresponding to the stability limit region for the ECS ($\hbar = \hbar^{\mathrm{crit}} = 1.6$) for which this scheme is showing constant oscillations. For this value, the corresponding maximal value of ω to ensure convergence of the iterative process is $\omega \approx 1.03$. The relative tolerance used is $\epsilon_{\mathrm{rel}} = 10^{-4}$. Several computations confirm the predicted behavior of the ICS : as long as ω stays under the calculated maximum value 1.03, the ICS converges toward the same smooth solution given by fig. 6a. Even for values $\hbar > \hbar^{\mathrm{crit}}$, the ICS handles smoothly the fast dynamics and important transient initiated by the instant propagation of the discontinuities at boundaries in the two domains by the LP models. For cases where the ECS is not
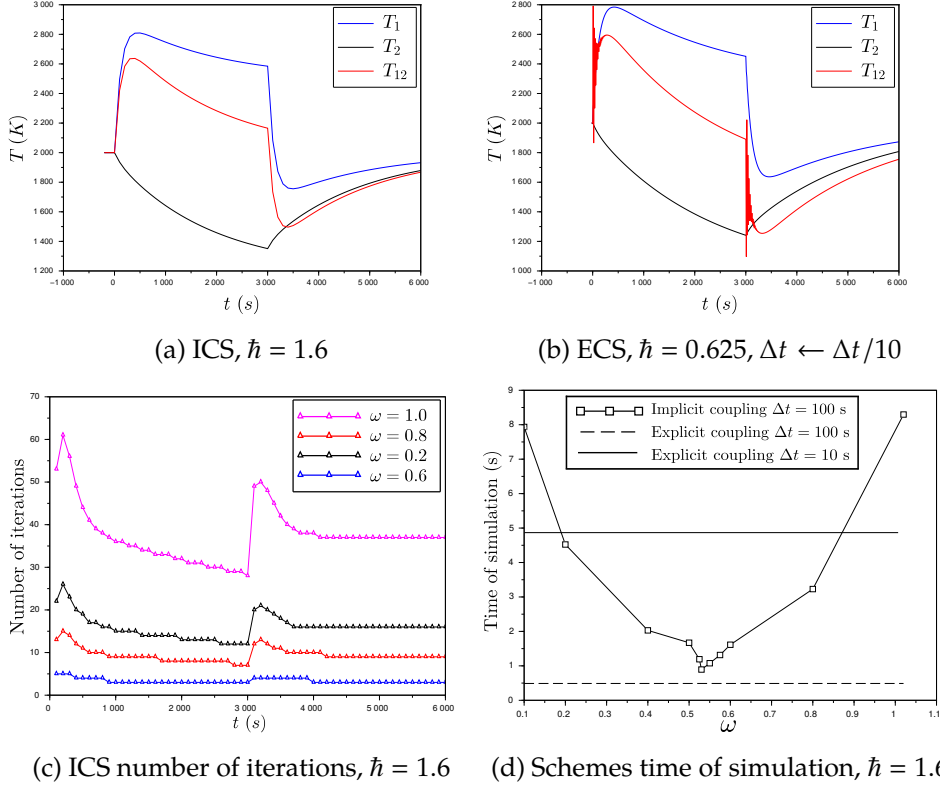
(a) ICS, $\hbar = 1.6$

(b) ECS, $\hbar = 0.625$, $\Delta t \leftarrow \Delta t/10$

(c) ICS number of iterations, $\hbar = 1.6$

(d) Schemes time of simulation, $\hbar = 1.6$

Figure 6: Propagation of discontinuities at boundaries of lumper parameter heat conduction coupled solvers solved with an ICS (upper left) and an ECS (upper right) with much smaller coupling time step.

unconditionally unstable, i.e. $r_{12}(\Delta t) < 1$, one way to achieve stability is to reduce the coupling time step : fig. 6b shows an explicit coupling solution with $\hbar = 0.625 < \hbar^{\mathrm{crit}} \approx 1$ and coupling time step Δt reduced by a factor of 10. However, while effectively reducing the oscillations, using an ECS with such a small coupling time step leads to higher computational time. The ICS allows to keep a sufficiently large coupling time step and a limited number of iterations as shown in figs. 6c and 6d. In the last figure, it is important to understand that only the solution given by the ECS with a small coupling time step is usable but is costly to obtain while the solution given with the ICS is good and costs 5 times less. For this problem, the optimal relaxation parameter leading to the higher convergence rate can be analytically calculated from eq. (41) and is given by $\omega = 1/(1 + r_{12}(\Delta t)) \approx 0.52$. However, most of the time the optimal relaxation parameter is highly dependent to the problem.

Figure 7: Internal states of domain Ω_2 and their transition functions.

4.2 Synchronization on internal events

For instance, let us describe the state of domain Ω_2 into a graph of three states as depicted in fig. 7 : *Heating*, *Melting* and *Empty* states. A state transition occurs when a certain algebraic function is activated, e.g. $\dot{m}_{21} < 0$. As explained section 3.2, each state has its own solver, its own set of equations and its own interface and boundary conditions. State transitions can lead to discontinuities of state or interface variables. For this case, equations of solver $\mathcal{M}^{\text{Heating}}$ are the ones described previously in section 4.1 while solver $\mathcal{M}^{\text{Melting}}$ continuous equations are given by

$$
\begin{cases}
\phi_{21} = \lambda_1 \dfrac{6T_2 - 4T_{21} - 2T_{b_2}}{e_2} & \text{in } \Omega_2 \\[2mm]
\dfrac{dm_2}{dt} = \rho_2 \dfrac{de_2}{dt} = -\dot{m}_{21} & \text{in } \Omega_2 \\[2mm]
\rho_2 C p_2 e_2 \dfrac{dT_2}{dt} = -\phi_{21} & \text{in } \Omega_2,
\end{cases}
\tag{44}
$$

leading to a mobile fusion solidification front at interface Γ_{12} given by eqs. (4) to (6) $\phi_{12} = -\phi_{21} + \Delta \mathcal{H}^{\text{fus.}} \dot{m}_{21}$, $\dot{m}_{12} = -\dot{m}_{21}$ and $T_{12} = T_{21} = T^{\text{fus.}}$. Again, another set of internal and boundary equations are used for solver $\mathcal{M}^{\text{Empty}}$ leading to a fixed interface given by eqs. (7) to (9) $\dot{m}_{12} = -\dot{m}_{21} = 0$, $T_{12} = T_{21}$, $\phi_{12} = -\phi_{21}$.

Again, at $t = 0^-$, both domains are at an equilibrium temperature of $T_1 = T_2 = T_{21} = T_{b_1} = T_{b_2} = 2000$ K. In particular, domain Ω_2 is in *Heating* state. At $t = 0^+$, $T_{b_1} = 3000$ K and $T_{b_2} = 3000$ K to force the *Melting* state transition when T_{21} reaches $T^\star = 2100$ K at time $t^\star_{H \to M}$. Once this state has been reached, the second domain is in *Melting* state until only a residual mass $m_2 = m^\epsilon = 150$ kg is left (corresponding to height $e_2 = 1.5$ cm) and the *Empty* state is reached at time $t^\star_{M \to E}$. The computation then stops when domain Ω_1 reaches a near stationary state. In addition, all of the computations use the value $\tau_2 = 10^4$ s, $\tau_1 = 8 \times 10^3$ s and different values for the time step Δt. The chosen values ensure that the ECS is stable, i.e. $r_{12}(\Delta t) < 1.0$. Table 1 shows the times of the internal events of domain Ω_2 computed by the ECS and the ICS for several coupling time steps. Usually, we ask the coupling time step to be bounded by

$$
\tau/10 = 800 \text{ s} \geq \Delta t \geq \tau/100 = 80 \text{ s} \quad \text{with} \quad \tau = \min(\tau_1, \tau_2)
$$

22

Δt (s)		100	50	25	10	1
	$r_{12}(\Delta t)$			< 1.0		
ECS	m_1^∞ (kg)	1492	1413	1347	1260	1256 †
	T_1^∞ (K)	1710	1708	1705	1702	1700 †
ICS	m_1^∞ (kg)	1255			1255	
	T_1^∞ (K)	1700			1700	
ECS	$t_{H\to M}^\star$ (s)	1700	1600	1600	1590	1584 †
	$t_{M\to E}^\star$ (s)	3200	3200	3150	3120	3117 †
ICS	$t_{H\to M}^\star$ (s)	1583			1583	
	$t_{M\to E}^\star$ (s)	3120	3117	3117	3116	3116

Table 1: Times $t_{H\to M}^\star$ and $t_{M\to E}^\star$ of domain Ω_2 internal events and stationary state m_1^∞ and T_1^∞ reached by domain Ω_1. Reference solution marked with †, solutions respecting the coupling time step constraint in blue, otherwise in red.

for computational efficiency (in red and blue in the table). In comparison to the reference solution (marked with †) given by the ECS for a small time step $\Delta t = 1$ s for which the scheme has converged, the ICS is able to predict the state transition with high accuracy and adapt its time step to synchronize both domains when the event occurs. However, the synchronization mechanism of the ECS only allows the domains to be informed of an event at the end of the time step. During this window of time, both domains are in a non physical state, i.e. the domain Ω_1 is not aware of the disappearance of the domain Ω_2. This leads to numerical errors of order $O(\Delta t)$ and the numerical creation of either mass and/or energy leading to different stationary states for the ECS. For a time step $\Delta t = 100$ s respecting the constraint, the explicit solution leads to a relative error of 18% in term of mass. Reducing the coupling time step to 10 s leads to a relative error of 0.3% but, as seen previously, increases computational time. Besides, the ICS always converges toward the reference solution and the right stationary state even for large coupling time step.

This very simple example of coupling of LP models highlights the main drawback of such lightweight modeling : deleting spatial dependency in the equations force each model to instantly propagate all its data, e.g. its discontinuities or its state transitions, thus creating high and important transient or bringing the system in non physical states. Fixes are used to bring back the system in a coherent state which should be avoided at all cost. These phenomenons create numerical errors in the coupling which can be measured in term of numerical energy created at the interface Γ_{12}.

We follow the same methodology as in [29]. The local variation of energy $\Delta E^{n\rightarrow n+1}$ at interface Γ_{12} between times t^n and t^{n+1} is the sum of the energy $\Delta E_1^{n\rightarrow n+1}$ send by domain Ω_1 through the interface and the energy $\Delta E_2^{n\rightarrow n+1}$ send by domain Ω_2 through the interface. For the continuous case in which both domains are strongly coupled, the local variation of energy is null. It is defined by equation

$$\Delta E^{n\rightarrow n+1} = \Delta E_1^{n\rightarrow n+1} - (-\Delta E_2^{n\rightarrow n+1})$$
$$= \int_{t^n}^{t^{n+1}} \phi_{12} - \left(\int_{t^n}^{t^{n+1}} \phi_{21} - \Delta\mathcal{H}^{\text{fus.}}\dot{m}_{21} \right)$$
$$= 0.$$

The global energy $\Delta E^{0\rightarrow n}$ through interface Γ_{12} is defined by

$$\Delta E^{0\rightarrow n} = \sum_{k=0}^{n} \Delta E^{k\rightarrow k+1} = 0 \tag{45}$$

and is also null in the continuous case. For each energy variation ΔE, we define the relative energy

$$\epsilon(\Delta E) = \frac{\Delta E}{E^\star} = \frac{\Delta E}{m_2(t^0)C_{p_2}(T^{\text{fus.}} - T_2(t^0)) + \Delta\mathcal{H}^{\text{fus.}}m_2(t^0)}$$

by the ratio of the energy ΔE to the energy $E^\star$ needed to heat the initial domain Ω_2 to its fusion temperature ($m_2(t^0)C_{p_2}(T^{\text{fus.}} - T_2(t^0))$) and to melt it ($\Delta\mathcal{H}^{\text{fus.}}m_2(t^0)$). With the physical values used, we have $E^\star \approx 10^8$ J.

When discretized for the ECS, the local variation of energy becomes

$$\Delta E^{n\rightarrow n+1} \approx \phi_{12}(t^{n+1})\Delta t - \left(\phi_{21}(t^n) - \Delta\mathcal{H}^{\text{fus.}}\dot{m}_{21}(t^n) \right)\Delta t$$

which emphasizes the "time-lag" between the two domains. Figure 8a shows that the ECS can create locally 2.5% of $E^\star$, i.e. $2.5\,10^6$ J. Figure 8b shows first that the global energy is not null and that terms of the sum eq. (45) do not sum to zero. Besides, the explicit scheme can create globally more than 6% of $E^\star$, i.e. $6\,10^6$ J which can have disastrous effects on the whole accuracy.

For the ICS, the local variation of energy becomes

$$\Delta E^{n\rightarrow n+1} \approx \phi_{12}(t^{n+1,\infty})\Delta t - \left(\phi_{21}(t^{n+1,\infty}) - \Delta\mathcal{H}^{\text{fus.}}\dot{m}_{21}(t^{n+1,\infty}) \right)\Delta t$$

in which variables with superscript ∞ represent the value reached when the convergence criterion of the iterative scheme is satisfied. At convergence, we can bound the residual at interface in such a way that

$$\left| \phi_{12}(t^{n+1,\infty}) - \left(\phi_{21}(t^{n+1,\infty}) - \Delta\mathcal{H}^{\text{fus.}}\dot{m}_{21}(t^{n+1,\infty}) \right) \right|\Delta t \leq \epsilon_{\text{rel}}\left| \phi_{12}(t^{n+1,\infty}) \right|\Delta t.$$
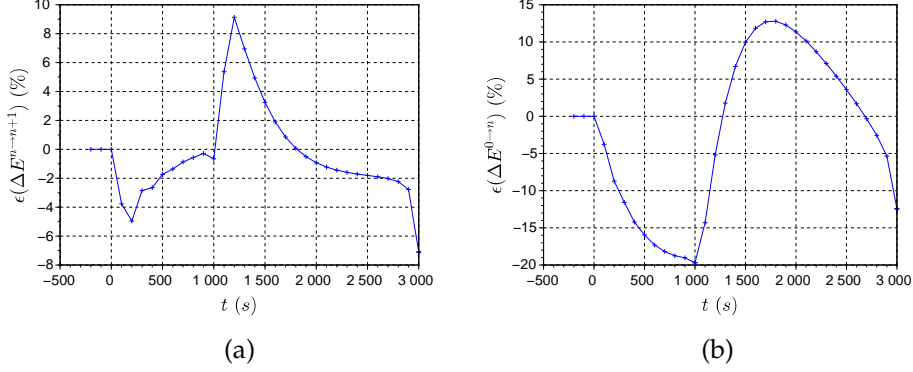
Figure 8: Relative local energy variation (*left*) and global energy variation (*right*) at interface for the ECS

This allows us to bound the relative local energy at interface of the ICS with

$$\left|\epsilon(\Delta E^{n\to n+1})\right| = \left|\frac{\Delta E^{n\to n+1}}{E^\star}\right| \leq \epsilon_{\text{rel}} \frac{\left|\phi_{12}(t^{n+1,\infty})\right|\Delta t}{E^\star}$$

and the relative global energy with

$$\left|\epsilon(\Delta E^{0\to n})\right| \leq \sum_{k=0}^{n} \left|\frac{\Delta E^{k\to k+1}}{E^\star}\right| \leq n\,\epsilon_{\text{rel}} \frac{\max_k \left|\phi_{12}(t^{k+1,\infty})\right|\Delta t}{E^\star}.$$

This shows that the imbalance of energy at interface of the ICS can be controlled with the relative tolerance ϵ_{rel}. This is confirmed by numerical experiments presented fig. 9a and fig. 9b showing respectively the relative local and global energy at interface with a relative tolerance set to 10^{-4}. The maximum heat flux $\max_k \left|\phi_{12}(t^{k+1,\infty})\right|$ reached at the interface with unit area is equal to $\approx 1.5 \times 10^5$ W.m^{-2} leading to a bound for the relative local energy at interface of 1.5×10^{-3} (expressed in percent in fig. 9a).

5 Conclusion and perspectives

In this paper, we have presented problems of coupled LP models with time management of state change events. In comparison to finer modeling approaches (e.g. mesh based modelings), this approach allows for fast calculations which are needed when doing statistical studies with a large number of calculations (e.g. design of computer experiments, Monte-Carlo methods). This is typically the true industrial context of modeling and simulation of severe accidents in nuclear reactors. However, we have shown that the LP modeling approach often leads to coupled problems with stiff,
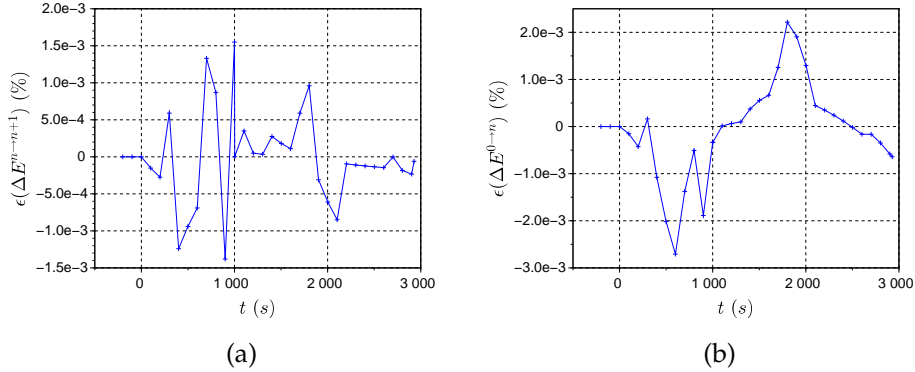
Figure 9: Relative local energy variation (*left*) and global energy variation (*right*) at interface for the ICS

important and fast transients which are not suitable for being solved by ECSs. Thus, ICSs were presented and designed for proper events detection and models synchronization allowing to obtain stable and accurate solutions of coupled problems of lumped parameter models.

We proposed to study theoretically the numerical stability of ECSs and ICSs on some of the interface equations used with LP models calculating the heat conduction in coupled domains. From this short study we have learned that Dirichlet-Neumann boundary conditions should be set up carefully in order to ensure stability of the coupling schemes. However with industrial constraints on the coupling time step to ensure fast calculations, ECSs remain very unstable and cannot be reasonable candidates in general cases to give good and precise results. Besides, even the cheapest ICSs that only use relaxation can give precise and stable calculations leading to trustworthy results. They turn out ot be very interesting in term of computational times in comparison to ECSs with a highly reduced coupling time step to ensure stability. Furthermore, the designed ICSs are able to predict events and discontinuities in the coupled models allowing synchronization between them. This tends to suggest that industrial problems of coupled lumped parameter models could substantially benefit from the use of implicit coupling schemes.

In future developments, it would be worthwhile to add *smartness* to the coupling scheme. For instance, depending on the strength of a coupling, i.e. the value of the residual at interfaces, the coupling scheme sould be able to choose between an ECS or an ICS to avoid using potentially costly iterative scheme. Indeed, we have seen that such schemes can be optimized to ensure fast calculations but this is still highly problem dependent. In particular this can be very useful in the context of statistical studies where the experiments are run into an automated process. Finally, if ICS are required to ensure

26

proper stability of the computation but are still too costly, time parallelism techniques like *parareal* methods [23] could be used.

6 Acknowledgments

References

[1] A. C. Aitken, *XXV.—On Bernoulli's Numerical Solution of Algebraic Equations*, Proceedings of the Royal Society of Edinburgh, 46 (1927), pp. 289–305, `https://doi.org/10.1017/S0370164600022070`, `https://www.cambridge.org/core/journals/proceedings-of-the-royal-society-of-edi` (accessed 2017-10-06).

[2] N. Boccara, *Modeling Complex Systems*, Graduate Texts in Physics, Springer New York, New York, NY, 2010, `https://doi.org/10.1007/978-1-4419-6562-2`.

[3] J. M. Bonnet and J. M. Seiler, *Thermohydraulic phenomena in corium pool: the BALI experiment*, in Proc. of ICONE 7, Tokyo, Japan, 1999.

[4] P. Causin, J. F. Gerbeau, and F. Nobile, *Added-mass effect in the design of partitioned algorithms for fluid–structure problems*, Computer Methods in Applied Mechanics and Engineering, 194 (2005), pp. 4506–4527, `https://doi.org/10.1016/j.cma.2004.12.005`, `http://www.sciencedirect.com/science/article/pii/S0045782504005328` (accessed 2017-04-25).

[5] J. Degroote, K.-J. Bathe, and J. Vierendeels, *Performance of a new partitioned procedure versus a monolithic procedure in fluid–structure interaction*, Computers & Structures, 87 (2009), pp. 793–801, `https://doi.org/10.1016/j.compstruc.2008.11.013`, `http://linkinghub.elsevier.com/retrieve/pii/S0045794908002605` (accessed 2016-08-09).

[6] J. Degroote and J. Vierendeels, *Multi-level quasi-Newton coupling algorithms for the partitioned simulation of fluid–structure interaction*, Computer Methods in Applied Mechanics and Engineering, 225–228 (2012), pp. 14–27, `https://doi.org/10.1016/j.cma.2012.03.010`, `http://www.sciencedirect.com/science/article/pii/S0045782512000862` (accessed 2017-03-22).

[7] V. Dolean, P. Jolivet, and F. Nataf, *An Introduction to Domain Decomposition Methods*, Other Titles in Applied Mathematics, Society for Industrial and Applied Mathematics, Nov. 2015, https://doi.org/10.1137/1.9781611974065.

[8] C. Farhat, M. Lesoinne, and N. Maman, *Mixed explicit/implicit time integration of coupled aeroelastic problems: Three-field formulation, geometric conservation and distributed solution*, International Journal for Numerical Methods in Fluids, 21 (1995), pp. 807–835, https://doi.org/10.1002/fld.1650211004/full.

[9] C. Farhat, K. C. Park, and Y. Dubois-Pelerin, *An unconditionally stable staggered algorithm for transient finite element analysis of coupled thermoelastic problems*, Computer methods in applied mechanics and engineering, 85 (1991), pp. 349–365, http://www.sciencedirect.com/science/article/pii/004578259190102C (accessed 2016-04-01).

[10] C. Farhat, A. Rallu, K. Wang, and T. Belytschko, *Robust and provably second-order explicit–explicit and implicit–explicit staggered time-integrators for highly non-linear compressible fluid–structure interaction problems*, International Journal for Numerical Methods in Engineering, 84 (2010), pp. 73–107, https://doi.org/10.1002/nme.2883.

[11] C. Farhat and N. Sobh, *A consistency analysis of a class of concurrent transient implicit/explicit algorithms*, Computer methods in applied mechanics and engineering, 84 (1990), pp. 147–162, http://www.sciencedirect.com/science/article/pii/0045782590901142 (accessed 2017-04-25).

[12] C. A. Felippa and K. C. Park, *Staggered transient analysis procedures for coupled mechanical systems: formulation*, Computer Methods in Applied Mechanics and Engineering, 24 (1980), pp. 61–111, http://www.sciencedirect.com/science/article/pii/0045782580900407 (accessed 2016-08-09).

[13] V. Ganine, N. J. Hills, and B. L. Lapworth, *Nonlinear acceleration of coupled fluid–structure transient thermal problems by Anderson mixing*, International Journal for Numerical Methods in Fluids, 71 (2013), pp. 939–959, https://doi.org/10.1002/fld.3689.

[14] J.-F. Gerbeau and M. Vidrascu, *A Quasi-Newton Algorithm Based on a Reduced Model for Fluid-Structure Interaction Problems in Blood Flows*, ESAIM: Mathematical Modelling and Numerical Analysis, 37 (2003), pp. 631–647, https://doi.org/10.1051/m2an:2003049.

[15] M. B. Giles, *Stability analysis of numerical interface conditions in fluid-structure thermal analysis*, International Journal for Numerical Methods in Fluids, 25 (1997), pp. 421–436, `https://doi.org/10.1002/(SICI)1097-0363(19970830)25:4<421::AID-FLD557>3.0.CO;2-`

[16] H. Guillard and C. Farhat, *On the significance of the geometric conservation law for flow computations on moving meshes*, Computer Methods in Applied Mechanics and Engineering, 190 (2000), pp. 1467–1482, `https://doi.org/10.1016/S0045-7825(00)00173-0`, `http://www.sciencedirect.com/science/article/pii/S0045782500001730` (accessed 2016-08-09).

[17] D. Jacquemain, *Les accidents de fusion du coeur des réacteurs nucléaires de puissance: état des connaissances (French)*, Collection sciences et techniques, EDP sciences, Les Ulis, 2013.

[18] M. M. Joosten, W. G. Dettmer, and D. Perić, *Analysis of the block Gauss-Seidel solution procedure for a strongly coupled model problem with reference to fluid-structure interaction*, International Journal for Numerical Methods in Engineering, 78 (2009), pp. 757–778, `https://doi.org/10.1002/nme.2503`.

[19] C. Kassiotis, A. Ibrahimbegovic, R. Niekamp, and H. G. Matthies, *Nonlinear fluid–structure interaction problem. Part I: implicit partitioned algorithm, nonlinear stability proof and validation examples*, Computational Mechanics, 47 (2011), pp. 305–323, `https://doi.org/10.1007/s00466-010-0545-6`.

[20] U. Küttler and W. A. Wall, *Fixed-point fluid–structure interaction solvers with dynamic relaxation*, Computational Mechanics, 43 (2008), pp. 61–72, `https://doi.org/10.1007/s00466-008-0255-5`.

[21] R. Le Tellier, L. Saas, and F. Payot, *Phenomenological analyses of corium propagation in LWRs: the PROCOR software platform*, in Proc. of the 7th European Review Meeting on Severe Accident Research ERMSAR-2015, Marseille, France, 2015.

[22] R. Le Tellier, E. Skrzypek, and L. Saas, *On the treatment of plane fusion front in lumped parameter thermal models with convection*, Applied Thermal Engineering, 120 (2017), pp. 314–326, `https://doi.org/10.1016/j.applthermaleng.2017.03.108`, `http://www.sciencedirect.com/science/article/pii/S1359431116327119` (accessed 2017-04-10).

[23] Y. Maday and G. Turinici, *The Parareal in Time Iterative Solver: a Further Direction to Parallel Implementation*, Springer

Berlin Heidelberg, Berlin, Heidelberg, 2005, pp. 441–448, https://doi.org/10.1007/3-540-26825-1_45.

[24] G. Mao and L. R. Petzold, *Efficient integration over discontinuities for differential-algebraic systems*, Computers & Mathematics with Applications, 43 (2002), pp. 65–79, https://doi.org/10.1016/S0898-1221(01)00272-3, http://www.sciencedirect.com/science/article/pii/S0898122101002723 (accessed 2017-06-21).

[25] M. Mehl, B. Uekermann, H. Bijl, D. Blom, B. Gatzhammer, and A. van Zuijlen, *Parallel coupling numerics for partitioned fluid–structure interaction simulations*, Computers & Mathematics with Applications, 71 (2016), pp. 869–891, https://doi.org/10.1016/j.camwa.2015.12.025, http://linkinghub.elsevier.com/retrieve/pii/S0898122115005933 (accessed 2016-08-09).

[26] C. Michler, E. H. van Brummelen, and R. de Borst, *An interface Newton-Krylov solver for fluid-structure interaction*, International Journal for Numerical Methods in Fluids, 47 (2005), pp. 1189–1195, https://doi.org/10.1002/fld.850.

[27] S. Minami and S. Yoshimura, *Performance evaluation of nonlinear algorithms with line-search for partitioned coupling techniques for fluid-structure interactions*, International Journal for Numerical Methods in Fluids, 64 (2010), pp. 1129–1147, https://doi.org/10.1002/fld.2274.

[28] L. Petzold, *Differential/Algebraic Equations are not ODE's*, SIAM Journal on Scientific and Statistical Computing, 3 (1982), pp. 367–384, https://doi.org/10.1137/0903023.

[29] S. Piperno and C. Farhat, *Partitioned procedures for the transient solution of coupled aeroelastic problems–Part II: energy transfer analysis and three-dimensional applications*, Computer methods in applied mechanics and engineering, 190 (2001), pp. 3147–3170, http://www.sciencedirect.com/science/article/pii/S0045782500003868 (accessed 2016-08-09).

[30] S. Piperno, C. Farhat, and B. Larrouturou, *Partitioned procedures for the transient solution of coupled aroelastic problems Part I: Model problem, theory and two-dimensional application*, Computer Methods in Applied Mechanics and Engineering, 124 (1995), pp. 79 – 112, https://doi.org/10.1016/0045-7825(95)92707-9, http://www.sciencedirect.com/science/article/pii/0045782595927079.

[31] I. Ramière and T. Helfer, *Iterative residual-based vector methods to accelerate fixed point iterations*, Computers & Mathematics with Applications, 70 (2015), pp. 2210–2226, https://doi.org/10.1016/j.camwa.2015.08.025, http://linkinghub.elsevier.com/retrieve/pii/S0898122115004046 (accessed 2017-01-16).

[32] B. R. Sehgal, *Nuclear safety in Light Water Reactors: Severe Accident Phenomenology*, Elsevier/Academic Press, Amsterdam ; Boston, 1st ed ed., 2012.

[33] J. Vierendeels, L. Lanoye, J. Degroote, and P. Verdonck, *Implicit coupling of partitioned fluid–structure interaction problems with reduced order models*, Computers & Structures, 85 (2007), pp. 970–976, https://doi.org/10.1016/j.compstruc.2006.11.006, http://www.sciencedirect.com/science/article/pii/S0045794906003865 (accessed 2017-05-05).

[34] L. Zhang, Y. Zhou, Y. Zhang, W. Tian, S. Qiu, and G. Su, *Natural convection heat transfer in corium pools: A review work of experimental studies*, Progress in Nuclear Energy, 79 (2015), pp. 167–181, https://doi.org/10.1016/j.pnucene.2014.11.021, http://www.sciencedirect.com/science/article/pii/S014919701400328X (accessed 2016-10-06).